www.serd.ait.ac.th/reric

Simulation of Flow Around and Behind a Savonius Rotor

M. Jaya Rajkumar, U. K. Saha and D. Maity*

Department of Mechanical Engineering
Indian Institute of Technology
Guwahati-781039
INDIA
*Department of Civil Engineering
Indian Institute of Technology
Guwahati-781039
INDIA

ABSTRACT

The fluid flow over a Savonius wind turbine rotor has been analyzed by using a multi-physics simulation program. The analysis accounts for fully flow simulation, the effect of rotation on flowfield in, around and far behind the turbine rotor. The aim of this investigation is to study the evolution of fluid contours and the velocity circulation. The flow distribution at various rotor tip speed ratios was studied at an air velocity of 10 m/s. Results obtained from the investigation have been discussed and analyzed.

1. INTRODUCTION

In order to design an efficient and high performance Savonius wind turbine, it is important to have a good understanding of how the design and the operating parameters affect the flow fields around the turbine. To clarify the power mechanism of the rotor, many researchers have investigated the flow field around a Savonius rotor, which is closely related to the torque and power performance of the rotor. Most investigations have been experimental studies with flow visualization techniques, such as smoke injection, smoke wire and water tunnel tests [1-3]. The present study focuses on using computer modeling to simulate the flow in, around and far behind the Savonius turbine, so as to obtain a sufficient insight into the flowfield. While structural analysts enjoy using powerful and matured finite element analysis (FEA) tools, fluid analysts are still handicapped with computational fluid dynamics (CFD) codes that require extensive knowledge of fluid mechanics. However, this situation is changing rapidly. First, significant advances in the fluid flow analysis made during recent years have brought about development of a number of commercial CFD codes, which are robust and efficient for general fluid flow analysis, and also user-friendly [4-10]. Additionally, efforts made recently have resulted in a very intelligent design of the user-interface such as providing efficient ways to create meshes, set modeling assumptions, and specify boundary conditions. These codes have been found increasingly useful in the process of product design. The Eulerian formulation in the fluid system can be solved by using a single program such as ADINA-F [11]. In this study, ADINA (automatic dynamic incremental non-linear analysis), a multi-physics simulation program, is used to model the fluid flow in, around and far behind the Savonius turbine. The analysis accounts flow distribution in, around and behind the turbine

2. DESCRIPTION OF THE PROBLEM

Figure 1 shows the computational domain of the 2-D Savonius wind turbine rotor with semicircular blade to be analyzed. The blockage ratio of the rotor is 0.54 in the flow plane. Flow enters the turbine rotor at 10 m/s. The computational domain has been solved first by keeping the rotor blade at 90^0

orientations in static position, and then in rotating condition with tip speed ratio (λ) of 1 for 0^0 and 90^0. The flow is assumed to be laminar and incompressible with a density of 1.205 kg/m^3 and a viscosity of 1.81 x 10^{-5} N-s/m^2 at a temperature of 20^0C. Boundary conditions are such that both the sidewalls are in no slip condition, and the flow is exiting to the atmosphere. The objective of this study is to simulate the fluid flow in, around and far behind the turbine rotor as described above, and in particular, examine the flow distribution under various rotational speeds.

3. MATHEMATICAL MODLES OF FLUID FLOW

The motion of a continuous fluid medium is governed by the principles of classical mechanics. In a rotating frame of reference, the non-conservative forms for mass and momentum equations can be expressed as

$$\frac{\partial \rho}{\partial \tau} + \nabla.(\rho V_r) = 0 \tag{1}$$

$$\frac{\partial \rho V_r}{\partial \tau} + \nabla.(\rho V_r V_r - \tau) = f^B + f^C \tag{2}$$

where τ is the time, r is the density, V_r is the relative velocity vector, f^B is the body force vector of the fluid, $\hat{\mathbf{o}}$ is the stress tensor, and adding the additional centrifugal force term f^C, called Coriolis force [11].

4. THE ADINA MODEL

It is to be noted that the flow simulation for the 3-D Savonius rotor is going to be CPU time intensive. The 3-D modeling is not feasible with the current computing resources. Moreover, as the rotor blades used in the present work are semicircular without any twist, the 2-D model will be capable of representing the flow behavior accurately as that of a 3-D model. Further, as the actual shape of the Savonius rotor is a projection of the 2-D plane only, this approximation will help to reduce the computational time. Therefore, in the 2-D simulation, the flow region is normally assumed to have a blade height normal to the computational domain. However, the results obtained are actually valid for any height, as there is no twist in these blades. The velocity and pressure fields from the 2-D modeling closely represent the 3-D situation. The amount of angular rotation to the centre depends on the case of study i.e., tip speed ratio.

In the present analysis, finite element analysis with ADINA-F, and no slip walls is used to model the channel. Boundary conditions used for the computational flow domain are shown in figure 1, while the meshes used are shown in figure 2. Pressure boundary conditions are imposed at the flow exit. Associated lines are introduced to limit the mesh region. Auxiliary lines and surfaces were used to further subdivide the computational domain in order to improve the mesh quality and make the mesh more robust. In order to simulate and compare the actual experimental condition, no slip condition to the sidewalls has been taken. Blockage ratio, as stated earlier, is kept at 0.54. This value closely relates wind tunnel tests with blockage ratio of around 0.64 [3]. The present fluid model built with the help of ADINA-F uses the available geometric data [12].

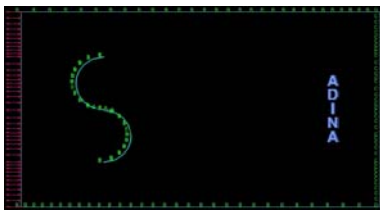

Fig. 1. Computational domain with boundary conditions.

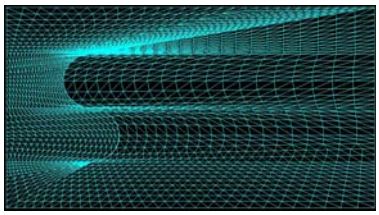

Fig. 2. A sufficiently refined ADINA mesh with sub divided surfaces.

5. COMPUTATIONAL RESULTS

Figures 3 and 4 show the velocity fields in the flow domain of the rotor at 90^0 orientation for static position (λ=0). The change in the flow fields due to orientation and rotation of the rotor can be clearly distinguished from these figures. The velocity vectors at 90^0 orientation of static blade are shown in figure 3. Flow velocity beside the convex side is higher than the other side, and a much (negative-reverse direction) lower velocity is found in the outer radius of vortex zone. In particle tracing plot (figure 4.), the shape of the wake formed behind the blade depends on the trailing shape of concave or convex side of the blade. Due to the concaveness, the flow is in reverse direction and a small region of vortex is formed, which can be seen from the plots.

In addition, recirculation flows (due to separation) are observed in some of flow regions of the flow domain. The back-flow is identified as a major factor that simulates coanda like flow pattern and may increase the turbine efficiency. This is due to reduction of pressure difference between concave and convex sides of returning blade, which in turn, reduce the negative torque developed by the returning blade. When the rotor is in static position, the wake behind the blade is too large as compared to the rotating condition. The triangles seen in figure 4 are the locations of the injectors that inject particles continuously to draw the path lines. The maximum velocity in the flow condition is found to be 29.29 m/s, while the minimum to be -11.42 m/s, i.e., in the vortex region.

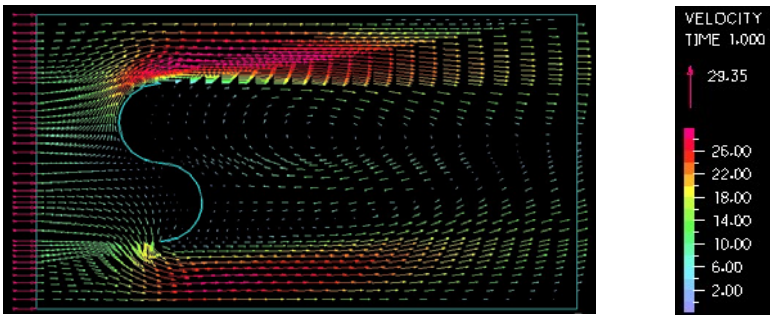

Fig. 3. Instantaneous velocity fields in whole domain.

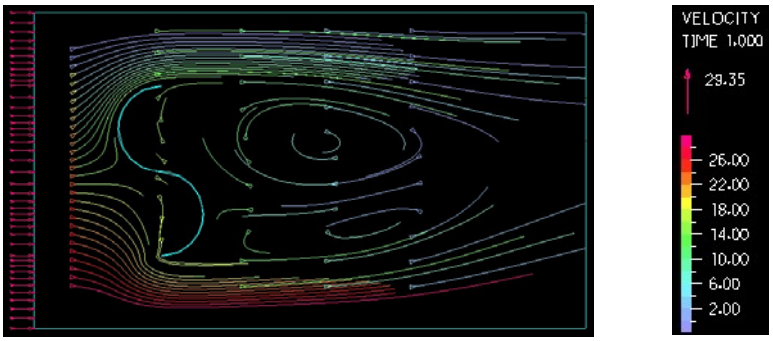

Fig. 4. Path lines of traced particles for static blade at 90^0 deg.

6. ROTATING CONDITION

The computational model outlined with both boundary conditions and an applied load is shown in figure 5. In the computational domain, a denser mesh has been generated near the rotor than at the front and far behind to capture better flow characteristics.

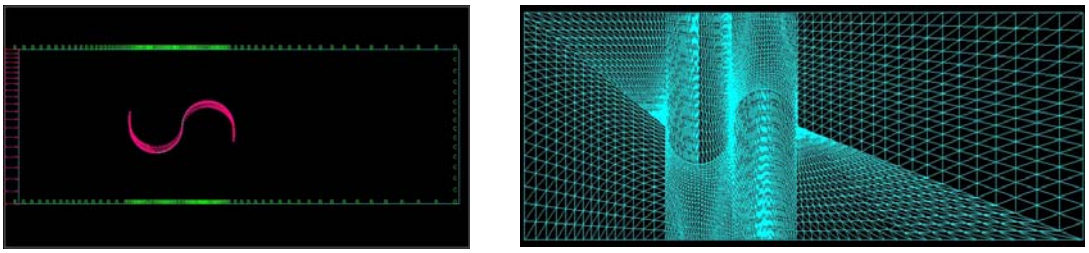

Fig. 5. Model domain with loads and boundary condition and a sufficiently refined ADINA mesh with subdivided surfaces.

The velocity vectors at 0^0 orientation of rotating blade are shown in figure 6. The flow velocity beside the convex side is found to be higher than the concave side. In particle tracing plot (figure 7), there is no strong wake for this flow configurations unlike the one with 90^0 orientation. The curvature of the front blade and the anticlockwise rotation of the rotor causes a high velocity zone just below the convex side with a maximum velocity of 25.4 m/s and minimum velocity is -5.095 m/s. The bands plot at 0^0 orientation of rotating blade is shown in figure 8.

Figure 9 represents the stream function of the rotating blade at 0^0 showing its maximum and minimum values of 15.65 and -13.01 respectively. As stream function represents a family of streamlines, therefore, a change in stream function corresponds to a change in flow rate, which in turn indicates the direction of flow.

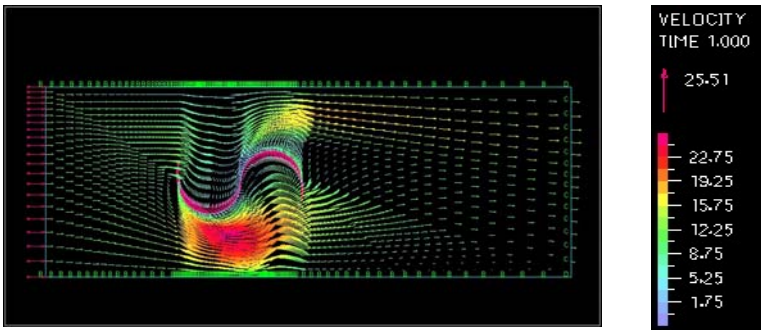

Fig. 6. Instantaneous velocity fields in whole domain with rata range.

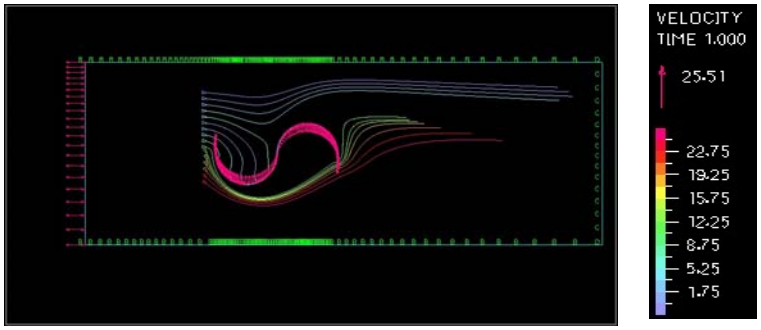

Fig. 7. Path lines of traced particles for rotating blade at 0^0 deg.

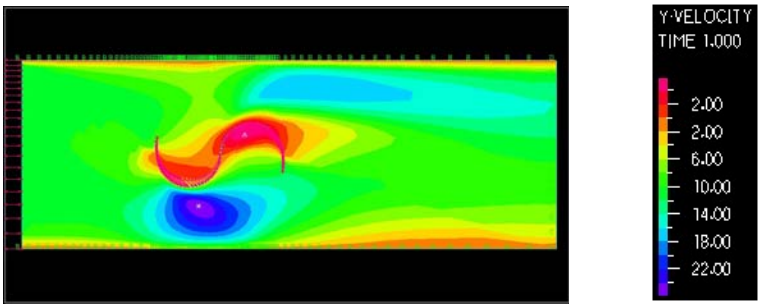

Fig. 8. Y velocity with load and boundary conditions at 0^0 deg.

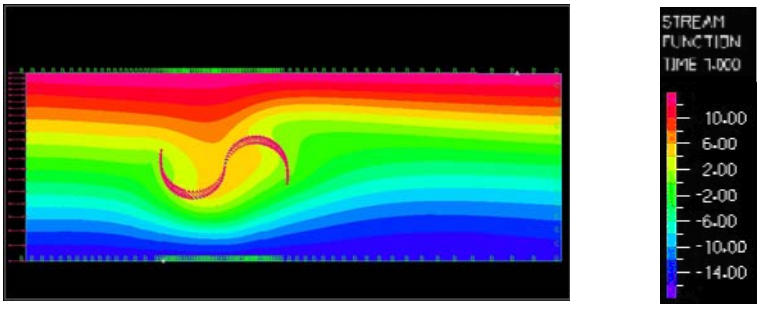

Fig. 9. Stream function with maximum 15.65 and minimum -13.01.

The velocity vectors at 90^0 orientation of rotating blade are shown in figure 10. It is seen that the flow velocity below the retuning blade is found to be higher than the advancing blade. The curvature of the returning blade and the rotation of the rotor in anticlockwise direction causes a high velocity zone just below the returning blade giving a maximum velocity of 26.98 m/s and minimum of –10.15 m/s. In the particle tracing plot (figure 11), there is a strong wake for these flow configurations unlike the one with 0^0 orientation. It can be seen that the particles pulled towards the concave side of the returning blade creates a strong wake behind the rotor. The velocity band and the stream function plots for the 90^0-rotating blade are shown in figures 12 and 13. The maximum and minimum values of fluid parameters obtained under various orientations and rotations are summarized in table 1.

Table 1. Summary of Results

Sl no	Parameter	Condition	Max	Min
1	Velocity	Static 0^0	11.66	0
		Static 90^0	29.29	-11.42
2	Stream function	Static 0^0	17.85	-10.52
		Static 90^0	19.88	-16.26
3	Velocity	Rotation 0^0	25.4	-5.095
		Rotation 90^0	26.98	-10.15
4	Stream function	Rotation 0^0	15.65	-13.01
		Rotation 90^0	18.63	-18.14

7. CONCLUSIONS

In the present investigation, the fluid flow over a Savonius rotor is analyzed using a multi-physics simulation program. In order to reduce the computing time, the model of the rotor is simplified into a 2-D case. The fluid flow equations are solved by the ADINA-F system. For a Savonius rotor in the stationary mode, the flow patterns around the rotor for upstream and downstream have been computed for an orientation angle of 90°, whereby the following points could be summarized.

1. Neither the rotor blade nor the incident flow is symmetric with respect to the horizontal plane. So no wake symmetry was obtained.
2. The flow to the returning bucket is partly due to induction effects from the upstream rotor and partly due to the airflow washed out from the advancing blade.
3. For rotor orientation angle of 90^0, the downstream flow is directed upwards i.e., towards the center of the rotor and the angularity in the downstream flow is weaker as compared to the upstream.

The main features of the induced flow field in the case of the running rotor are:

1. Due to the rotation of the rotor, the flowstreams are deflected in the same sense as the spinning rotor. As such the flow patterns will differ from those for the stationary rotor as observed in figures 4 and 11.
2. The flow swirls at the rotor tips due its rotation and the flow moving downstream will combine and disturb the flow significantly in the wake region.
3. Vortex behind the rotor is strong enough to hold a larger area of recirculation.

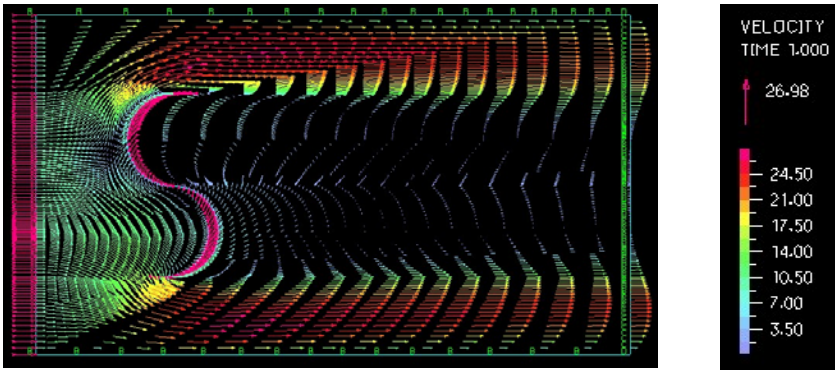

Fig. 10. Instantaneous velocity fields in domain with data range for rotating blade at 90^0 deg.

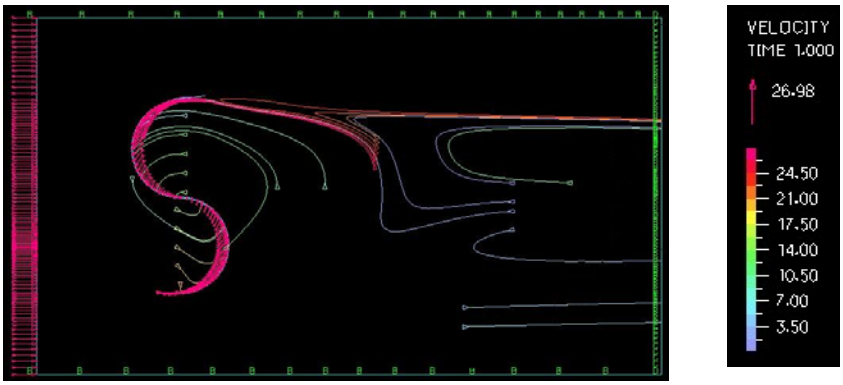

Fig. 11. Path lines of traced particles for rotating blade at 90^0 deg.

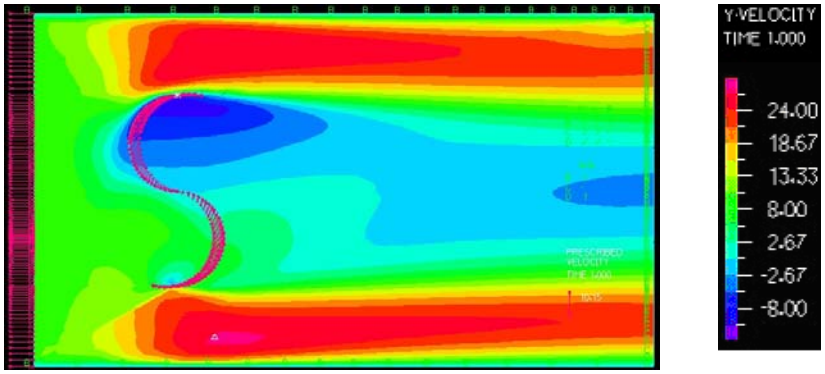

Fig. 12. Velocity band plot with boundary condition and loads with data range.

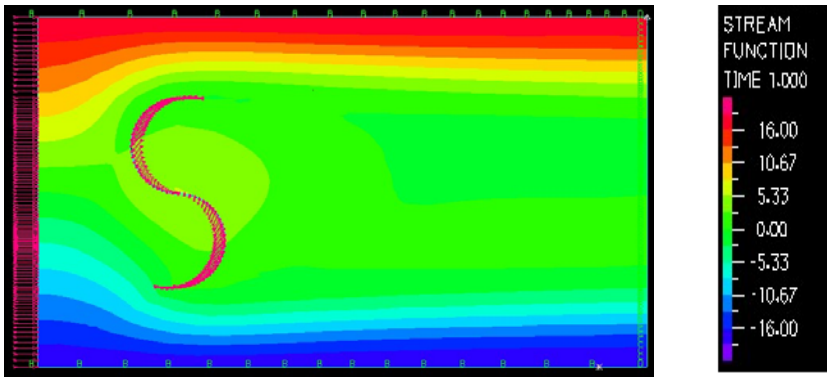

Fig. 13. Stream function with values of maximum 18.63 and minimum –18.14.

8. REFERENCES

[1] Mojola, O. O., (1985), "On The Aerodynamics Design of The Savonius Windmill Rotor," Journal of Wind Engineering and Industrial Aerodynamics, Vol .15, pp. 223-231.

[2] Modi, V. J., and Fernando, M. S. U. K., (1989), "On the Performance of the Savonius Wind Turbine," ASME Journal of Solar Energy Engineering, Vol. 111, pp.71-81.

[3] Fujisawa, N., and Gotoh, F., (1992), "Pressure Measurement and Flow Visualization Study of Savonius Rotor" Journal of Wind Engineering and Industrial Aerodynamics, Vol .39, pp. 51-60.

[4] Xiaoqing, Z., Joe Z. L. and Mike, R., (2000), "Flow Simulation of a Direct-Injection Gasoline Diaphragm Fuel Pump with Structural Interactions," SAE Technical Paper Series-2000-01-1047.

[5] Bathe, K. J., Zhang, H., and Zhang, X., (1997), "Some Advances in the Analysis of Fluid Flows," Computers and Structures, Vol. 64, pp. 909-930.

[6] C., Freitas, (1995), "Perspective: Selected Benchmarks from Commercial CFD Codes," ASME Journal of Fluids Engineering, Vol. 117, pp. 208-218.

[7] Bathe, K.J., Zhang, H., and Wang, M.H., (1995), "Finite Element Analysis of Incompressible and Compressible Fluid Flows with Free Surfaces and Structural Interactions," Computers and Structures, Vol. 56, pp. 193-213.

[8] Kotb, M. A., and Aldoss, T. K., (1991), "Flow Field Around a Partially-Blocked Savonius Rotor, Applied Energy, Vol. 38, pp.117-132.

[9] Bathe, K.J., (1996), "Simulation of Structural and Fluid Flow Response in Engineering Practice," Computer Modeling and Simulation in Engineering, Vol. 1, pp. 47-77.

[10] Bathe, K.J., Zhang, H., and Ji, S., (1999), "Finite Element Analysis of Fluid Flows Fully Coupled with Structural Interactions," Computers and Structures, Vol. 72, pp. 1-16.
[11] ADINA R & D, Inc., (2003), "ADINA-F Theory and Modeling Guide," Report No. ARD-03-9.
[12] Huda, M. D., Selim, M. A., Sadrul Islam, A. K. M., and Islam, M. Q., (1992),"The Performance of an S-shaped Savonius Rotor with a Deflecting Plate," RERIC International Energy Journal, Vol. 14, pp.25-32.